Heritage Science

RESEARCH

Open Access

Characteristic burn temperature markers of bones as revealed by electron paramagnetic resonance

Tilen Knaflič[1,2*], Lea Legan[2], Fabio Cavalli[3] and Polonca Ropret[2,4]

Abstract

This research paper presents a novel methodology for determining the burn temperature of archaeological bones using electron paramagnetic resonance (EPR) supported by Fourier Transform Infrared (FTIR) spectroscopy. A selection of bone samples, burned at different temperatures, were examined with EPR. The EPR spectra displayed dependency on burn temperature, showing characteristic narrow spectra of carbon radicals, Mn^{2+} signals and signals from different carbonate ions. This methodology was applied to selected archaeological samples of burnt bones, successfully determining the burn temperature these bones were exposed to in the past. The extracted burn temperatures showed good agreement with those determined from a complementary reflectance FTIR study.

Keywords Burnt bones, EPR spectroscopy, Burn temperature, Reflection FTIR spectroscopy, Archaeological bones, Thermal degradation

Introduction

Archaeological remains often show signs of exposure to elevated temperatures. This can vary in intensity from a mild exposure, which in most cases affects only the appearance, to extreme exposure that can change chemical composition of the remains and can even render the object unrecognizable. Studying such objects often leads to attempts to determine the temperature they were exposed to. This can provide valuable information on the source of exposure and thus enable the researcher to gain insight into the historical context on what has transpired at a specific archaeological site. Most common events are different burial rituals, natural disasters, armed conflicts, meal preparation, etc. [1–6].

These events affect organic matter to a much higher degree than other materials, therefore human, animal or plant remains show more significant changes when exposed to elevated temperatures. From this group, bones are a very common archaeological find and the exposure of bones to these kind of conditions causes different physical and chemical changes in them. The most vivid physical observation after bones' exposure to high temperatures is colour change. At the lowest burn temperatures, we observe charring of the organic component with the change of colour from white to black. With increasing temperature, the black colour then slowly changes to grey and finally it becomes white (Table 1 and Ref. [7]). Beside the colour change, different processes and transformations (i.e. charring, mineral recrystallization, microscopic cracking and shrinkage, etc.) also take place during the heat exposure, regarding its core components collagen and carbonate hydroxyapatite. The latter bone component, together with other present trace

*Correspondence:
Tilen Knaflič
tilen.knaflic@ijs.si
[1] Condensed Matter Physics Department, Jožef Stefan Institute, Jamova 39, 1000 Ljubljana, Slovenia
[2] Research Institute, Institute for the Protection of Cultural Heritage of Slovenia, Poljanska 40, 1000 Ljubljana, Slovenia
[3] Research Unit of Paleoradiology and Allied Sciences, Universitary Integrated Health Care, 34100 Trieste, Italy
[4] Faculty for Chemistry and Chemical Technology, University of Ljubljana, Večna pot 113, 1000 Ljubljana, Slovenia

Table 1 Sample labels with respect to their burn conditions (burn time and temperature)

T (°C)	30 min	60 min	90 min	120 min
300	S2 (b)	S3 (b)	S4 (b)	S5 (b)
600	S6 (b)	S7 (bg)	S8 (bg)	S9 (bg)
900	S10 (bw)	S11 (gw)	S12 (gw)	S13 (w)
1200	S14 (bw)	S15 (bw)	S16 (w)	S17 (w)

In the parentheses next to the labels are letters, describing the different colours of the sample (*b* black, *g* grey and *w* white). The raw (unheated) sample is labelled S1

elements and molecules, may be subjected to many substitutions during heat exposure. Elevated temperatures therefore change atomic order and the size of the apatite crystal, while the proportion of the organic matrix gradually decreases [2, 4, 7–12].

Determination of burn temperatures based on change of colour or detailed surface examination is in most cases insufficient and is subjected to large uncertainties [13–15]. To provide better burn temperatures of archaeological bones, a technique that also probes different structural, physical and chemical changes in the bones is needed [16]. FTIR spectroscopy is a useful and versatile technique for monitoring the state of burnt bones [2, 4, 8–12]. Recently, Legan et al. [7] showed a great potential of reflection Fourier-transform infrared (FTIR) spectroscopy in non-invasive manner for studying archaeological burnt bones. The study first included investigation on experimentally heated bones where total reflection spectra disclose specific thermal degradation products of bones, such as α and β-tricalcium phosphate, calcium pyrophosphate, aromatic compounds, etc. Collected FTIR spectra also reveal distinctive peaks, which belong to characteristic anionic and cationic substitutions. These isomorphic ion replacements are distinctive for bioapatite due to its crystal structure and presence of various ions in its formula [17].

The exposure of organic matter to elevated temperatures usually creates various paramagnetic centres and radicals, which can be detected by the means of the electron paramagnetic resonance (EPR). In the past, EPR has been extensively used to study coal and other similar materials, which are rich in carbon-based radicals [18–22]. These types of radicals also appear in different charred remains, often in archaeological context, thus making EPR a very suitable technique to study them [23–27]. Very recently, a detailed study of archaeological bones using EPR found correlations of stable carbon and nitrogen isotope ratios and *g*-factor with burn temperature [28]. They concluded that some information about the burn temperature could be extracted, however the accuracy is limited by the age of the studied sample. Besides the organic matter, the burning of other materials also produces different paramagnetic species, such as those observed in burned ceramics, where interesting elemental substitutions of manganese and calcium in $CaCO_3$ was detected and analysed [29, 30].

The aim of this study is to investigate the possibility of determining the burn temperature of bones by studying their EPR spectra. This is done by performing EPR measurements on bone samples, which were burned in laboratory conditions at known temperatures. The proposed EPR methodology, combined with the complementary FTIR spectroscopy analysis is then applied on burnt bones from archaeological context in order to determine their burn temperature.

Methods

Samples

For the purpose of this study, we used the right femoral diaphysis of adult cattle, which was defleshed using a sharp knife and carefully freed from the periosteum and bone marrow. It was then sawed using a butcher's band saw into 17 pieces of approximately the same size of 4.5 cm × 4 cm. The resulting fragments were placed in a large ceramic capsule and placed in the oven once the desired temperature was reached. 16 samples were thus exposed to different burn conditions, regarding temperature and time of exposure, one was left as a reference. The sample labels with regards to those two parameters are presented in Table 1. The same samples were previously used in the reflection FTIR study of experimentally burnt bones [7].

EPR spectroscopy

Room temperature X-band EPR measurements were done using the benchtop EPR spectrometer Bruker EMXnano with microwave frequency of 9.63 GHz. For this purpose, small same-coloured parts of the burnt bone samples were extracted using a scalpel and inserted into 4 mm Suprasil quartz tubes. Therefore, one initial bone sample could contribute up to three different coloured samples for EPR measurements (Table 1). For selected samples, additional low-temperature measurements between room temperature and 4 K were conducted using a Bruker Elexsys E580 X-band spectrometer operating at 9.37 GHz and equipped with a Varian TEM104 dual-cavity resonator, Oxford Instruments ESR900 cryostat and an Oxford Instruments ITC503 temperature controller with temperature stability better than ± 0.05 K. The burnt bone samples were measured more than a year after they were burned.

FTIR reflection spectroscopy

Archaeological burnt bones were examined with portable Alpha-R spectrometer (Bruker Optics, Germany). Contactless and non-destructive FTIR analysis were performed with external reflection module and 25°/25° optical layout. The total reflection spectra of archaeological burnt bones were collected in the spectral range between 8000 and 375 cm^{-1}, with 4 cm^{-1} spectral resolution. Five spectra were acquired for each sample and an average of 160 spectral scans were accumulated. We refer the reader to our previous manuscript for the methodology [7].

Results and discussion

Firstly, we measured the reference sample (S1), which was not exposed to elevated temperatures. EPR spectra of sample S1 appears at $g = 2.0047$ as a weak Gaussian line of width $\Delta B = 0.73$ mT (Fig. 1a top). The narrow EPR linewidth and g-factor close to the free electron value $g_e = 2.0023$ indicate, that the EPR signal is most probably of free radical origin [31, 32]. In contrast to FTIR spectroscopy, in which collagen, lipids and calcium hydroxyapatite are clearly resolved, it is difficult to determine the exact origin of an EPR signal in heterogeneous materials such as bone. The free radicals that produce the observed EPR signal in our reference bone sample S1, are most probably formed on organic parts of the bone due to broken bonds or other defects, that can occur during various degradation processes or mechanical stress [33, 34]. In the case of free radicals, we usually expect to see a Lorentzian lineshape of the EPR signal, instead we observe a Gaussian line. This could mean either an electron–electron dipolar interaction or an unresolved hyperfine interaction between the electron and a nearby nucleus [35]. The former option is more plausible, since the long-range nature

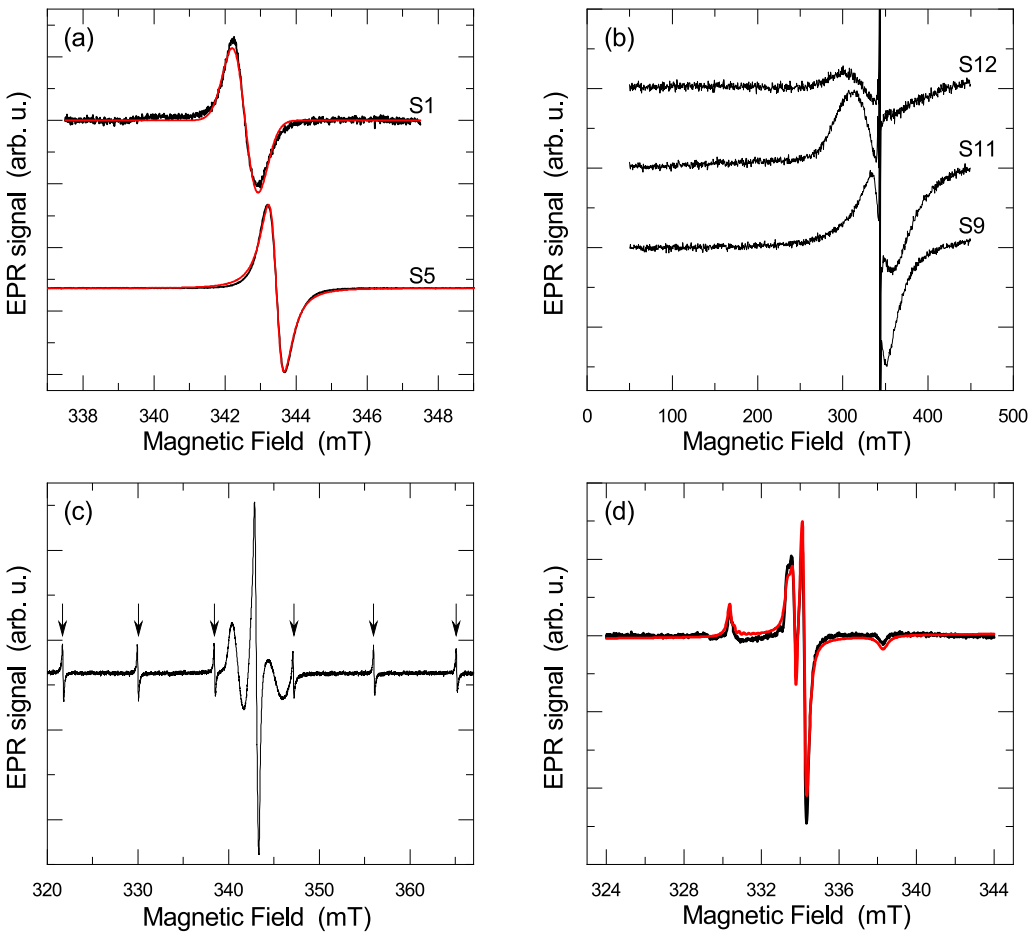

Fig. 1 Examples of EPR spectra, characteristic for different colours found in the bone samples: (**a**-top) sample S1—raw (unheated) bone acquired after 45 scans, (**a**-bottom) sample S5 (black)—burned for 120 min at 300 °C, **b** grey samples S9 (120 min, 600 °C), S11 (60 min, 900 °C) and S12 (90 min, 900 °C), **c** White sample S13 (120 min, 900 °C). Marked with six arrows are EPR lines corresponding to electron hyperfine interaction with $I = 5/2$ nuclear spin of Mn^{2+}. **d** EPR spectra of white parts of the bone of sample S11 measured at 4 K (black line), fitted by a three-component powder spectrum simulation with g-factor anisotropy

Table 2 Experimental data for the *g*-factor, EPR linewidth (ΔB) and spin concentration (n_s) for the black parts of the burnt bone samples

Sample	T (°C)	Time (min)	*g*-factor	ΔB (mT)	n_s (10^{13} mg^{-1})
S2	300	30	2.00455	1.24	0.05
S3	300	60	2.00357	0.88	4.7
S4	300	90	2.00326	0.78	23
S5	300	120	2.00329	0.76	14
S6	600	30	2.00330	0.72	13
S7	600	60	2.00330	0.68	13
S8	600	90	2.00298	0.67	21
S9	600	120	2.00303	0.67	15
S10	900	30	2.00314	0.27	52
S14	1200	30	2.00233	0.39	16
S15	1200	60	2.00277	0.62	1.84

of the dipolar interaction and the measured low spin concentration of $n_s = 1.2 \cdot 10^{11}$/mg support the case of random diluted defects.

The black parts of the burnt bone samples all have very similar EPR spectra. The relatively strong signal appears as a narrow Lorentzian line positioned around $g \approx 2$ (Fig. 1a bottom). The spectra were fitted to a single isotropic Lorentzian lineshape, the results of the fits are presented in Table 2. The *g*-factor and EPR linewidth values suggest the EPR signals are of free radical origin, more specifically carbon radicals [24, 36–40], which are formed when organic matter is exposed to high temperatures. The same type of radicals are also found in charcoal and coal [18–22]. The data presented in Table 2 is in good agreement with the *g*-factor and EPR linewidth values found in the literature, thus further confirming the presence of carbon radicals in our burnt bone samples. The charring effect is visible also in reflection FTIR spectra collected on bones heated up to 300 °C [7].

The change in bone colour from black to grey first appears in samples that were burned at 600 °C. The grey parts of the bones were carefully separated from the rest and put into the EPR quartz sample tubes. The measured EPR signal is qualitatively very similar to the EPR spectrum of black parts of the bone, shown in Fig. 1a, with the narrow Lorentzian lineshape and $g \approx 2$. This indicates the same origin of the EPR signal – carbon based free radicals. The only difference is in the spin concentration, which is noticeably lower than in the case of the black parts of the bone (Table 3). Additionally, in grey parts of the bones of samples S9, S11 and S12, very broad EPR spectra with $g = 1.993$ (S9, 600 °C) and $g \approx 2.01$ (S11 and S12, 900 °C) are observed (Fig. 1b). The measured EPR spectra are also characterized by the broad linewidth that spans from

Table 3 Experimental data for the *g*-factor, EPR linewidth (ΔB) and spin concentration (n_s) for the grey parts of the burnt bone samples

Sample	T (°C)	Time (min)	*g*-factor	ΔB (mT)	n_s (10^{13} mg^{-1})
S7-1	600	60	2.00351	0.73	7.9
S8-1	600	90	2.00328	0.73	7.1
S9-1	600	120	2.00339	0.69	5.6
S11	900	60	2.00269	0.36	5.6
S12	900	90	2.00267	0.37	9.7

35 to 80 mT with increasing burn temperatures. The origin of these spectra is unknown, with transition metals like iron (Fe) or manganese (Mn) being the best candidates. Even though it is known that both Fe and Mn, and also many other elements, are present naturally in bones [41–44], their concentration is too low to explain this broad signal. The calibrated EPR signal intensity provides an estimate for the concentration of approximately 2 percent, if the signal would originate from Mn or Fe. This is a few orders of magnitude too much, since the concentration in bones for both Fe and Mn are expected to be in the ppm range [41–44].

At the highest burn temperatures, we find that the majority colour of the burnt bone samples turns to white (Table 1). The measured EPR spectra on white parts of the bones (from here on referred to as white spectra) differ significantly, when compared to the simple EPR spectra observed before for the case of black and grey parts. The white spectra consist of a complex central set of EPR lines and an additional set of six narrow lines, equally separated by 8.5 mT (Fig. 1c). These six lines indicate hyperfine coupling of the $S = 1/2$ electron spin to the $I = 5/2$ nuclear spin of Mn^{2+}. Since we did not detect the Mn^{2+} signal at lower burn temperatures, it must have changed its oxidation state from a non-magnetic one to 2+, most probably it is substituting calcium in $CaCO_3$. This process was observed before in ceramics, and since $CaCO_3$ is present in bones, it could also be what is occurring in our case [29, 30]. Furthermore, the complementary reflection FTIR spectroscopy analysis also detected this substitution taking place at 900 °C [7].

To characterize the central complex set of EPR signals of the white bone parts, we cooled the sample down to liquid helium temperatures (4.2 K) and measured the EPR spectrum. We observe the shape of the EPR spectrum is characteristic of that of multiple components with *g*-factor anisotropy (Fig. 1d). After a careful analysis of the spectra, we find that three components are needed to describe the EPR signal in full detail, one

Table 4 Results from S11 sample EPR spectra simulation with *g*-factor anisotropy at 4.3 K

Source	g_x	g_y	g_z	I/I_0
CO_2^-	1.9794	2.0055	2.0264	1
CO_3^{3-}	2.0063	2.0063	2.0088	0.09
$C^{\bullet -}$	2.0035	2.0035	2.0035	0.21

Listed are *g*-factor values and relative intensities, where $I_0 = 3.88$.

isotropic Lorentzian line, one with axial *g*-factor anisotropy and another with rhombic *g*-factor anisotropy (Table 4). The isotropic component is either carbon based radical or some defect-based radical. The possibility of the signal being of carbon radical origin though is low, since at such high burn temperatures, the carbon radicals are usually gone. The most possible candidates for the other two components, based on the *g*-factors' values and anisotropy type, are CO_2^- and CO_3^{3-} [45, 46].

In order to now try and extract the burn temperature of bones from the EPR data, we first analyse the results from the EPR spectra of carbon-based radicals. In Fig. 2(top), we plot the measured *g*-factor values from Tables 2 and 3 versus burn temperature. We observe a general trend of decreasing *g*-factor values with increasing temperature. At each temperature there is some spread in the data due to different times of exposure. The same type of plot of EPR linewidth ΔB shows a similar trend Fig. 2(bottom). This information can be used to make an estimate on burn temperature based on the EPR signal of carbon radicals, that we find in burnt archaeological bones. To get the best estimates possible, the studied archaeological sample would have to be burned again at different temperatures, starting from low temperatures and then progressing up to higher temperatures, with EPR measurements done at room temperature after every step. We would expect that EPR measurements done after burning the sample at temperatures lower than the original burn temperature, would produce signals with fairly constant values of *g*-factor and EPR linewidths. Only after we would exceed the original burn temperature, would we notice a change, a decrease, in these two EPR parameters[28, 47]. This is possible due to the fact that the *g*-factor and EPR linewidth are highly dependent on their local crystal-field surroundings, which change irreversibly each time a bone is burned at a certain temperature. Therefore, when we expose the archaeological bone sample again to lower temperatures than the original, this does not induce changes in the local crystal-field surroundings of the radical, only when we go above the original burn temperature is when we start to induce additional changes in the structure and in turn also in the *g*-factor and EPR linewidth values. This method can give

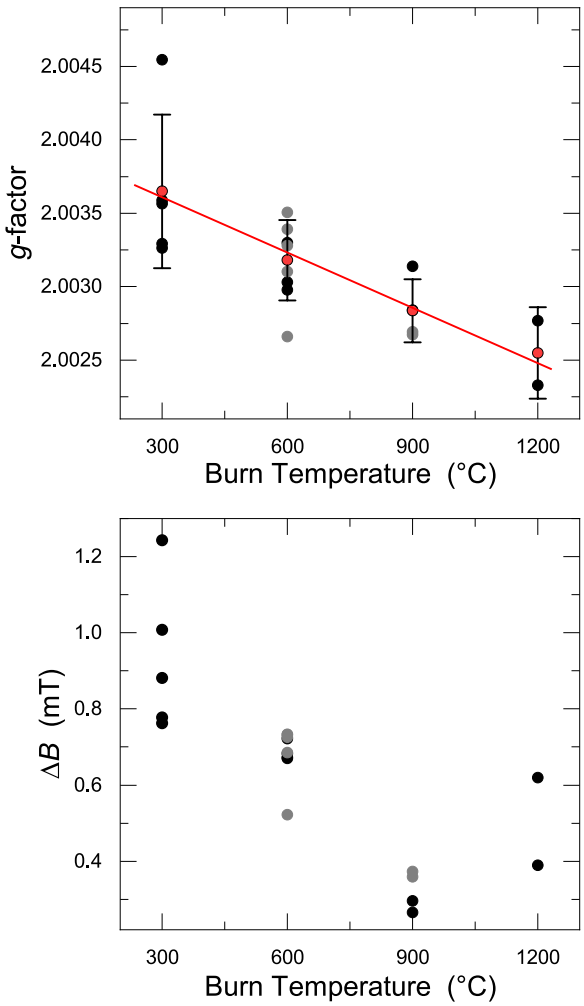

Fig. 2 Top: Dependence of *g*-factor values of carbon-based radicals on the burn temperature. Black circles represent data from black parts of the bone and grey circles from the grey parts of the bone. The red circles are the average *g*-factor values at a given burn temperature. The solid red line is a linear fit to the average *g*-factor values. Bottom: Dependence of EPR linewidth ΔB of carbon-based radicals on the burn temperature. Black circles represent data from black parts of the bone and grey circles from the grey parts of the bone

us relatively good burn temperature estimates, however the sample undergoes irreversible changes as it needs to be burned, sometimes extensively, above the original burn temperature. A much less accurate but indestructible way to obtain burn temperature estimates, is to use the data from Fig. 2(top) and (bottom) to make a simple model, for example a linear fit of the average *g*-factor values at each temperature, which can then be used to determine the burn temperature from the measured archaeological samples, together with some error estimates. We stress here that the *g*-factor values obtained for different times of exposure at selected burn temperatures

have large spread, which in turn causes the average values to have a large error associated to them. Therefore, the burn temperatures obtained from this simple model are useful only as very rough estimates.

The detection of the unknown broad resonance observed for burn temperatures of 600 °C and 900 °C can also serve us as a good marker for burn temperature estimates. From the detection of this signal, we can assume that the burn temperature could be in the range between 600 and 900 °C. Since we additionally observe, that these signals broaden with increasing burn temperature and shift to higher *g*-factor values, we could also get an estimate whether the burn temperature is more towards the lower or the upper boundary. We should note here, that this is a very rough approximation, for a more accurate determination of the burn temperature from *g*-factor and EPR linewidth of these broad signals, more burn temperature points should be taken in this range with more bone samples, to provide better statistics.

Another good marker for burn temperature estimates is the observed Mn^{2+} EPR signal in bones exposed to temperatures in the range between 900 and 1200 °C. Similarly, as written above, the detection of this characteristic signal points to the bone burn temperature in this temperature range. Additionally, the absence of this signal can also serve us as an indication that the bone burn temperature was below 900 °C.

Finally, we test the above-described EPR methodology on selected archaeological samples excavated from Slovenian archaeological site. The EPR results collected on burnt archaeological samples were compared with the validated results of reflection FTIR spectroscopy. All examined burnt bone fragments were excavated at archaeological site in Drnovo in southeast of Slovenia.

The EPR measurements of the archaeological burned bone sample labelled A1 show a wide Lorentzian line at $g = 2.05$ and $\Delta B \approx 85$ mT, together with 6 lines of Mn^{2+} of manganese-substituted calcium in $CaCO_3$ and the central set of lines, belonging to different carbonate radicals (Fig. 3a). This puts the burn temperature somewhere between 800 °C and 900 °C. The reflection FTIR spectrum (Fig. 3b) collected on sample A1 shows characteristic signals of carbonate vibrations placed at 1465 cm^{-1}, 1411 cm^{-1} and 873 cm^{-1}, which indicate a primarily carbonate substituted calcium apatite (i.e. B-type substitution) [48]. Carbonate anion forbidden bands are placed at 2928 cm^{-1}, 2509 cm^{-1} and 2464 cm^{-1}. These signals usually arise when bone is exposed to 900 °C for longer times. Absorbance bands of HCN2–, NCO–, CN22– groups of cyanamidapatite and/or calcium deficient cyanamidapatite are located at 3242 cm^{-1}, 2204 cm^{-1} and 2014 cm^{-1}, respectively. Furthermore, the reflection FTIR spectrum reveals distinct absorption bands of Cl–OH vibration at 3497 cm^{-1}, as well as the signal of 1st overtone of OH stretching at 6986 cm^{-1}. The latter two signals indicate that the bone sample A1 was exposed to at least 900 °C [7].

The second archaeological burned bone sample labelled A2 also shows an EPR spectrum consisting of a wide Lorentzian line at $g = 2.02$ and $\Delta B \approx 77$ mT, together with the 6 lines of Mn^{2+}, but without the central set of lines of carbonate radicals (Fig. 3c). Instead, only a single isotropic line, centred at $g = 2.0025$ and with $\Delta B \approx 0.34$ mT, that is most probably of carbon radical origin. The *g*-factor and linewidth values put the burn temperature at around 900 °C, which is also in line with the detected manganese and broad EPR signal. Figure 3d reports a reflection FTIR spectrum collected on the sample A2. ν_3 vibrations of carbonate groups are in the reflection FTIR spectrum placed at 1549 cm^{-1} and 1448 cm^{-1}. The latter band is in the FTIR spectrum slightly broadened and contains additional peak at 1402 cm^{-1}. The presence of all three signals of ν_3 vibrations of carbonate groups along with the presence of derivative-like ν_2 carbonate band ($\sim$ 872 cm^{-1}) suggesting the hydroxyl and carbonate substituted calcium apatite (i.e. AB-type substitution) [48]. Moreover, this spectrum contains a well-resolved $2\nu_3$ and $\nu_3 + \nu_1$ combination bands of carbonate anion placed at 2927 cm^{-1}, 2859 cm^{-1}, 2512 cm^{-1} and 2466 cm^{-1}. These signals are unmistakable in bones that have been exposed for a longer time, at least at a temperature of 900 °C. The exposure of this bone sample to a temperature of 900 °C is supported also by the detection of retained molecular CO_2 (IR band at $\sim$ 2347 cm^{-1}), a weak interaction between hydroxyl group and of Cl^- anion (IR band at $\sim$ 3497 cm^{-1}) and the presence of first overtone of the OH stretching vibrations in the near-IR region (IR band at $\sim$ 6969 cm^{-1}). Furthermore, the strong IR absorptions are visible in the region of overtones and combination bands. The bands at 2204 cm^{-1} and 2014 cm^{-1} along with the signal at 3242 cm^{-1}, confirm the presence of cyanates and cyanamides.

On another archaeological burned bone sample labelled A3, the EPR spectrum consists of a broad Lorentzian line at $g = 2.08$ and $\Delta B \approx 130$ mT, with an addition of a narrow Lorentzian line with $g = 2.0032$ and $\Delta B = 0.4$ mT (Fig. 3e). These values put the burn temperature, based on the narrow component, between 600 and 900 °C, which are in line with the detection of the broad EPR signal. Infrared reflection spectrum of sample A3 is illustrated in Fig. 3f. B-type substitution is indicated in the spectrum based on the vibration of carbonate anion placed at 1475 cm^{-1}, 1395 cm^{-1} and 875 cm^{-1}. The presence of carbonate anion is confirmed also by detection of typical doublet at 2509 cm^{-1} and 2466 cm^{-1}. Additional bands are present in the reflection spectrum placed at

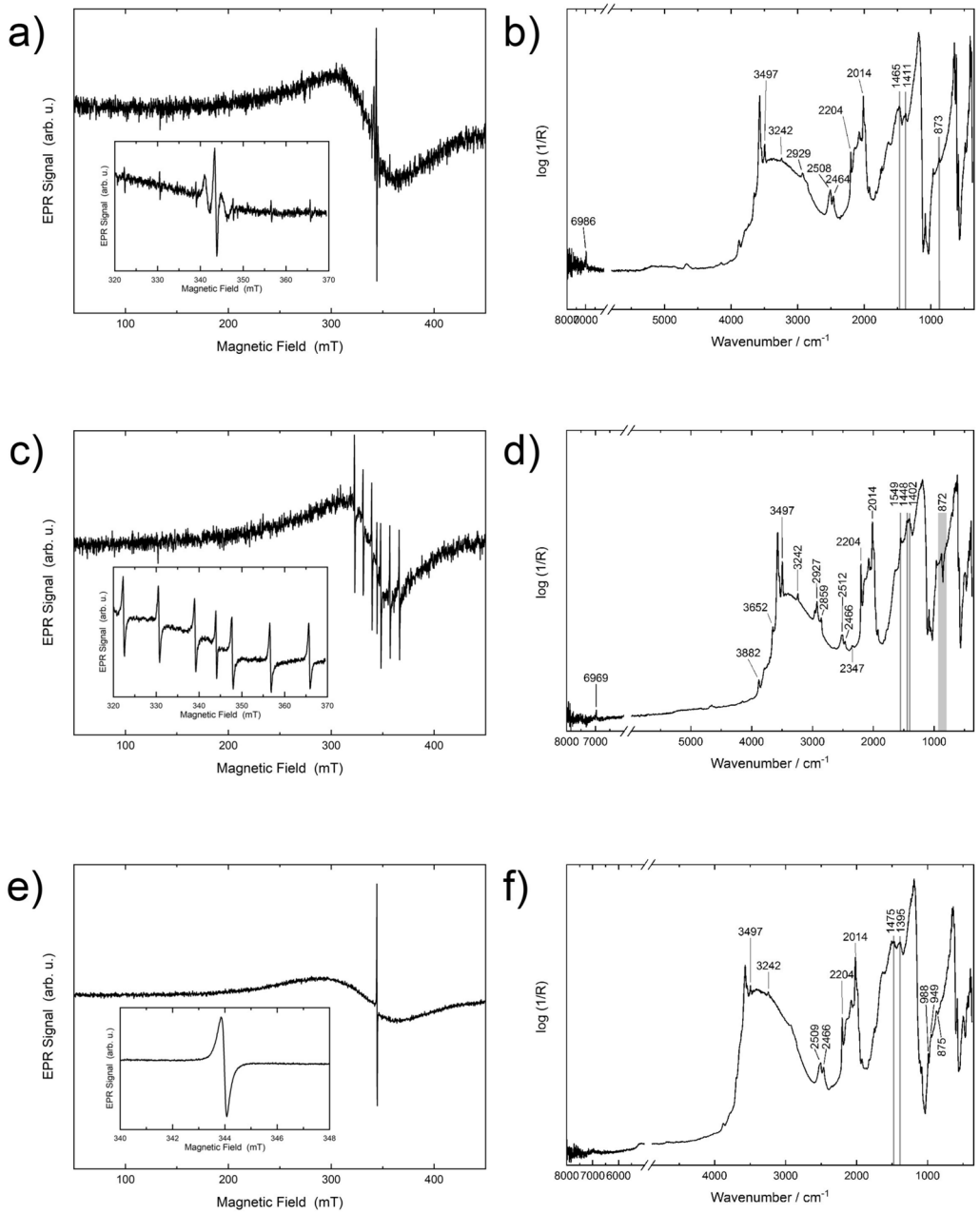

Fig. 3 EPR (**a**, **c** and **e**) and reflection FTIR (**b**, **d** and **f**) spectra for archaeological burnt bones samples labelled A1 (**a** and **b**), A2 (**c** and **d**) and A3 (**e** and **f**). The insets in the EPR plots show the details of the spectra in a narrow magnetic field range around $g \approx 2$

988 cm^{-1} and 949 cm^{-1}. These signals suggest the detection of β-tricalcium phosphate (β-TCP, $Ca_3(PO_4)_2^-$). β-TCP is a thermal degradation product of hydroxyapatite. Based on our previous research, the detection of β-TCP suggests that this bone fragment was exposed to a temperature of at least about 800 °C [49]. On the other hand, the reflection spectrum reveals also signals of Cl-OH vibration placed at 3497 cm^{-1} which is used as a marker that the bone was exposed to temperatures at least 900 °C. Cyanamideapatites are also detected in the corresponding FTIR spectrum, based on their typical absorptions at 3242 cm^{-1}, 2204 cm^{-1} and 2014 cm^{-1}.

Conclusions

The research conducted in this study is based on EPR measurements on model burnt bones samples, which were burned at controlled temperatures of 300 °C, 600 °C, 900 °C, and 1200 °C. The obtained results show

an interesting dependence of the measured EPR spectra on the burn temperatures, with characteristic carbon-based radical signals dominating the lower end of the burn temperatures, the emergence of the broad EPR signal of unknown origin in the mid-range burn temperatures, and Mn^{2+} and carbonate ions signals at higher temperatures. These different EPR signals can serve us as characteristic burn temperature markers and with a careful analysis of the obtained results, we were able to construct a novel model for determining an estimate for the burn temperature of bones based on the measured EPR spectrum. Finally, to test this methodology in practice, we employed it, together with a complementary reflection FTIR spectroscopy measurements, on different archaeological burned bone samples. The two methods provided us with similar burn temperature estimates and have thus confirmed that our EPR-based model performs well. The interdisciplinary approach of determining the burn temperature of archaeological bones with EPR and reflection FTIR spectroscopy can prove to be very useful in the future. The methods are relatively fast and easy to use, however the accuracy of the burn temperature estimates could be improved. In the future, additional studies are needed to improve on this by perhaps providing model burnt bone samples at more selected temperatures and also by employing additional complementary techniques, such as pulsed EPR or solid state NMR. Nevertheless, this research has opened up additional avenues for archaeological studies, providing a complementary understanding of historical events and practices. This study promises great potential for the use of EPR to determine the burn temperature of bones and adds another piece to the mosaic of archaeological research, bringing us one small step closer to unravelling the mysteries of our past.

Abbreviations

EPR Electron paramagnetic resonance
FTIR Fourier transform infrared spectroscopy

Acknowledgements

We would like to thank Asst. Prof. Tamara Leskovar and Asst. Prof. Matija Črešnar from the Faculty of Arts of University of Ljubljana, Slovenia, for providing the archaeological burnt bone samples. Additionally, we would like to thank dr. Dario Innocenti from Research Unit of Paleoradiology and Allied Sciences of Universitary Integrated Health Care in Trieste Italy, for providing the model burnt bone samples. This research was a part of IPERION HS that received funding from the European Union's Horizon 2020 research and innovation programme under Grant Agreement n. 871034. T. K. acknowledges financial support from the Slovenian Research Agency (Core Research Funding No. P1-0125).

Author contributions

T. K. performed EPR measurements, analysed and simulated EPR data, discussed the EPR and FTIR results, composed the burn temperature model, wrote and edited the manuscript. L.L. performed FTIR measurements, discussed the EPR and FTIR results, wrote and edited the manuscript. F. C. prepared the model burnt bones samples. P. R. conceived, developed and supervised the work and edited the manuscript. All authors read and approved the final manuscript.

Funding

This research was a part of IPERION HS that received funding from the European Union's Horizon 2020 research and innovation programme under Grant Agreement n. 871034. T. K. acknowledges financial support from the Slovenian Research Agency (Core Research Funding No. P1-0125).

Availability of data and materials

The datasets used and/or analysed during the current study are available from the corresponding author on reasonable request.

Declarations

Competing interests

The authors declare that they have no known competing financial interests or personal relationships that could have appeared to influence the work reported in this paper.

Received: 17 January 2024 Accepted: 10 May 2024
Published online: 22 May 2024

References

1. Bunch TE, LeCompte MA, Adedeji AV, Wittke JH, Burleigh TD, Hermes RE, et al. A Tunguska sized airburst destroyed Tall El-Hammam a Middle Bronze Age city in the Jordan Valley near the Dead Sea. Sci Rep. 2021;11(1):18632. https://doi.org/10.1038/s41598-021-97778-3.
2. Festa G, Rubini M, Zaio P, Gozzi A, Libianchi N, Parker S, et al. Vibrational spectroscopy to study ancient Roman funerary practices at the "Hypogeum of the Garlands"(Italy). Sci Rep. 2022;12(1):3707. https://doi.org/10.1038/s41598-022-07689-0.
3. Gowlett JA, Harris JW, Walton D, Wood BA. Early archaeological sites, hominid remains and traces of fire from Chesowanja, Kenya. Nature. 1981;294(5837):125–9. https://doi.org/10.1038/294125a0.
4. Festa G, Andreani C, Baldoni M, Cipollari V, Martínez-Labarga C, Martini F, et al. First analysis of ancient burned human skeletal remains probed by neutron and optical vibrational spectroscopy. Sci Adv. 2019;5(6):eaaw1292. https://doi.org/10.1126/sciadv.aaw1292.
5. Bazgir B, Ollé A, Tumung L, Becerra-Valdivia L, Douka K, Higham T, et al. Understanding the emergence of modern humans and the disappearance of Neanderthals: insights from Kaldar Cave (Khorramabad Valley, Western Iran). Sci Rep. 2017;7(1):43460. https://doi.org/10.1038/srep43460.
6. Stahlschmidt M, Mentzer S, Heinrich S, Cooper A, Grote M, McNeill P, et al. Impact of a recent wildfire on tortoises at Cape Point, South Africa, and implications for the interpretation of heated bones in the archaeological record. Archaeol Anthropol Sci. 2023;15(8):1–28. https://doi.org/10.1007/s12520-023-01806-4.
7. Legan L, Leskovar T, Črešnar M, Cavalli F, Innocenti D, Ropret P. Non-invasive reflection FTIR characterization of archaeological burnt bones: reference database and case studies. J Cult Herit. 2020;41:13–26. https://doi.org/10.1016/j.culher.2019.07.006.
8. Thompson T, Gauthier M, Islam M. The application of a new method of Fourier Transform Infrared Spectroscopy to the analysis of burned bone. J Archaeol Sci. 2009;36(3):910–4. https://doi.org/10.1016/j.jas.2008.11.013.
9. Gonçalves D, Thompson TJ, Cunha E. Implications of heat-induced changes in bone on the interpretation of funerary behaviour and practice. J Archaeol Sci. 2011;38(6):1308–13. https://doi.org/10.1016/j.jas.2011.01.006.
10. Piga G, Gonçalves D, Thompson TT, Brunetti A, Malgosa A, Enzo S. Understanding the crystallinity indices behavior of burned bones and teeth by ATR-IR and XRD in the presence of bioapatite mixed with other phosphate and carbonate phases. Int J Spectr. 2016;2016:1–9. https://doi.org/10.1155/2016/4810149.
11. Marques MP, Batista de Carvalho L, Gonçalves D, Cunha E, Parker S. The impact of moderate heating on human bones: an infrared and neutron spectroscopy study. R Soc Open Sci. 2021;8(10): 210774. https://doi.org/10.1098/rsos.210774.

12. Marques MP, Gonçalves D, Mamede A, Coutinho T, Cunha E, Kockelmann W, et al. Profiling of human burned bones: oxidising versus reducing conditions. Sci Rep. 2021;11(1):1361. https://doi.org/10.1038/s41598-020-80462-3.
13. Rosa J, Marques MPM, Gonçalves D, Ferreira MT. Half a century of systematic research on heat-induced colour changes in bone-a review. Sci Just. 2023. https://doi.org/10.1016/j.scijus.2023.07.002.
14. Martínez de Los Reyes PI, Gutiérrez A, Macho-Callejo A, García-Morato S, Moreno-García M, Fernández-Jalvo Y. Let's play with fire! Preliminary results of new experiments on animal bone of thermo-alterations. Hist Biol. 2023. https://doi.org/10.1080/08912963.2023.2258912.
15. Nicholson RA. A morphological investigation of burnt animal bone and an evaluation of its utility in archaeology. J Archaeol Sci. 1993;20(4):411–28. https://doi.org/10.1006/jasc.1993.1025.
16. Ellingham ST, Thompson TJ, Islam M, Taylor G. Estimating temperature exposure of burnt bone—a methodological review. Sci Just. 2015;55(3):181–8. https://doi.org/10.1016/j.scijus.2014.12.002.
17. Leroy N, Bres E, Jones D, Downes S. Structure and substitutions in fluorapatite. Eur Cells Mater. 2001;2(33):36–48. https://doi.org/10.22203/eCM.v002a05.
18. Petrakis L, Grandy D. Electron spin resonance spectrometric study of free radicals in coals. Anal Chem. 1978;50(2):303–8. https://doi.org/10.1021/ac50024a034.
19. Tadyszak K, Augustyniak-Jabłokow MA, Wieckowski AB, Najder-Kozdrowska L, Strzelczyk R, Andrzejewski B. Origin of electron paramagnetic resonance signal in anthracite. Carbon. 2015;94:53–9. https://doi.org/10.1016/j.carbon.2015.06.057.
20. Bresgunov AY, Dubinsky A, Poluektov O, Vorob'eva G, Lebedev YS. Electron paramagnetic resonance of coals. New approaches to an old problem with multifrequency electron paramagnetic resonance and spin echo. J Chem Soc Faraday Trans. 1990;86(19):3185–9. https://doi.org/10.1039/FT9908603185.
21. Duber S, Wieckowski AB. EPR study of molecular phases in coal. Fuel. 1982;61(5):433–6. https://doi.org/10.1016/0016-2361(82)90067-9.
22. Mrozowski S. ESR studies of carbonization and coalification processes part II. Biological materials. Carbon. 1988;26(4):531–41. https://doi.org/10.1016/0008-6223(88)90152-2.
23. Robins G, Del Re C, Seeley N, Davis A, Hawari JA. A spectroscopic study of the Nimrud ivories. J Archaeol Sci. 1983;10(4):385–95. https://doi.org/10.1016/0305-4403(83)90077-8.
24. Robins G. The study of heated and charred archaeological materials with electron spin resonance spectroscopy. J Anal Appl Pyrolysis. 1984;6(1):31–43. https://doi.org/10.1016/0165-2370(84)80003-0.
25. Ikoma T, Ito O, Tero-Kubota S. Exploring radicals in carbonaceous solids by means of pulsed EPR spectroscopy. Energy Fuels. 2002;16(1):40–7. https://doi.org/10.1021/ef010148j.
26. Smirnova TI, Smirnov AI, Clarkson R, Belford R. Half-field EPR transitions in synthetic carbohydrate chars. Solid State Commun. 1994;91(4):319–23. https://doi.org/10.1016/0038-1098(94)90309-3.
27. Emmerich F, Rettori C, Luengo C. ESR in heat treated carbons from the endocarp of babassu coconut. Carbon. 1991;29(3):305–11. https://doi.org/10.1016/0008-6223(91)90198-R.
28. Schurr MR, Hayes RG. Stable carbon-and nitrogen-isotope ratios and electron spin resonance (ESR) g-values of charred bones: changes with heating and a critical evaluation of the utility of g-values for reconstructing thermal history and original isotope ratios. J Archaeol Sci. 2008;35(7):2017–31. https://doi.org/10.1016/j.jas.2008.01.007.
29. Felicissimo MP, Peixoto JL, Bittencourt C, Tomasi R, Houssiau L, Pireaux JJ, et al. SEM, EPR and ToF-SIMS analyses applied to unravel the technology employed for pottery-making by pre-colonial Indian tribes from Pantanal, Brazil. J Archaeol Sci. 2010;37(9):2179–87. https://doi.org/10.1016/j.jas.2010.03.015.
30. Udomkan N, Limsuwan P. Aragonite to calcite transformation studies by Esr of Mn 2+ ions in Sinotaia Ingallsiana. Mod Phys Lett B. 2009;23(09):1243–7. https://doi.org/10.1142/S0217984909019375.
31. Weil JA, Bolton JR. Electron paramagnetic resonance: elementary theory and practical applications. John Wiley & Sons; 2007.
32. Spasojević I. Free radicals and antioxidants at a glance using EPR spectroscopy. Crit Rev Clin Lab Sci. 2011;48(3):114–42. https://doi.org/10.3109/10408363.2011.591772.
33. Corredor C, Diaz J, Diaz JM, Farach HA, Poole C. ESR experiments with egg shells of chickens. Appl Magn Reson. 1995;9(3):309–17. https://doi.org/10.1007/BF03161955.
34. Marino AA, BECKER RO. Mechanically induced free radicals in bone. Nature. 1968;218(5140):466–7. https://doi.org/10.1038/218466a0.
35. Poole CP, Farach HA. Line shapes in electron spin resonance. Bull Magn Reson. 1979;1(4):162–94.
36. Trubetskaya A, Jensen PA, Jensen AD, Glarborg P, Larsen FH, Andersen ML. Characterization of free radicals by electron spin resonance spectroscopy in biochars from pyrolysis at high heating rates and at high temperatures. Biomass Bioenergy. 2016;94:117–29. https://doi.org/10.1016/j.biombioe.2016.08.020.
37. Feng JW, Zheng S, Maciel GE. EPR investigations of charring and char/air interaction of cellulose, pectin, and tobacco. Energy Fuels. 2004;18(2):560–8. https://doi.org/10.1021/ef0301497.
38. Milsch B, Windsch W, Heinzelmann H. EPR investigations of charred cellulose. Carbon. 1968;6(6):807–12. https://doi.org/10.1016/0008-6223(68)90066-3.
39. Pilawa B, Wieckowski A, Pietrzak R, Wachowska H. Multi-component EPR spectra of coals with different carbon content. Acta Phys Polonica Ser A Gen Phys. 2005;108(2):403–8.
40. Green U, Shenberger Y, Aizenshtat Z, Cohen H, Ruthstein S. Exploring the radical nature of a carbon surface by electron paramagnetic resonance and a calibrated gas flow. J Vis Exp JoVE. 2014. https://doi.org/10.3791/51548.
41. Harkness JS, Darrah TH. From the crust to the cortical: the geochemistry of trace elements in human bone. Geochim et Cosmochimica Acta. 2019;249:76–94. https://doi.org/10.1016/j.gca.2019.01.019.
42. Buddhachat K, Klinhom S, Siengdee P, Brown JL, Nomsiri R, Kaewmong P, et al. Elemental analysis of bone, teeth, horn and antler in different animal species using non-invasive handheld X-ray fluorescence. PLoS ONE. 2016;11(5): e0155458. https://doi.org/10.1371/journal.pone.0155458.
43. Budis H, Kalisinska E, Lanocha N, Kosik-Bogacka D, Sokolowski S, Dobiecki K, et al. The concentration of manganese, iron, and strontium in hip joint bone obtained from patients undergoing hip replacement surgery. J Trace Elem Med Biol. 2014;28(1):39–44. https://doi.org/10.1016/j.jtemb.2013.07.004.
44. Fore H, Morton R. The manganese in bone. Biochem J. 1952;51(5):598. https://doi.org/10.1042/bj0510598.
45. Fattibene P, Callens F. EPR dosimetry with tooth enamel: a review. Appl Radiat Isotopes. 2010;68(11):2033–116. https://doi.org/10.1016/j.apradiso.2010.05.016.
46. Wencka M, Hoffmann S, Hercman H. EPR dating of hydroxyapatite from fossil bones. Transient Effects after gamma and UV irradiation. Acta Phys Polonica Ser A. 2005;108(2):331. https://doi.org/10.12693/APhysPolA.108.331.
47. Le Pape L. Application of EPR in studies of archaeological samples. Cham: Springer; 2016.
48. Madupalli H, Pavan B, Tecklenburg MM. Carbonate substitution in the mineral component of bone: discriminating the structural changes, simultaneously imposed by carbonate in A and B sites of apatite. J Solid State Chem. 2017;255:27–35. https://doi.org/10.1016/j.jssc.2017.07.025.
49. Mkukuma L, Skakle JMS, Gibson IR, Imrie CT, Aspden RM, Hukins DWL. Effect of the proportion of organic material in bone on thermal decomposition of bone mineral: an investigation of a variety of bones from different species using thermogravimetric analysis coupled to mass spectrometry, high-temperature X-ray diffraction, and Fourier transform infrared spectroscopy. Calcified Tissue Int. 2004;75:321–8. https://doi.org/10.1007/s00223-004-0199-5.

Publisher's Note